Numerical investigation of the effect of divergent hot tube on the energy separation in a vortex tube

Masoud Rahimi[1]*, Seyed Ehsan Rafiee[2], Nader Pourmahmoud[1]

[1]Department of Mechanical Engineering, Urmia University of Technology, Urmia, Iran
[2]Department of Mechanical Engineering, Kermanshah Branch, Islamic Azad University, Kermanshah, Iran
* m.rahimi@mee.uut.ac.ir

ABSTRACT

A mechanical device with no moving parts, a vortex tube can generate cold and hot gas flows from compressed gas. This paper investigates the effect of using a divergent hot tube on vortex tube refrigeration capacity. The computational fluid dynamics (CFD) model used is a three-dimensional steady compressible model utilizing the k-ε turbulence model. In this numerical research, different divergence angles of the hot tube (β=0°, 1°, 2°, 3°, 4°, and 6°) have been simulated to analyze the performance of the vortex tube. The results showed that as the angle diverges from β=0°, cold temperature separation improves at cold mass fractions greater than about 0.4, but increasing the angle to more than 4° impairs cold temperature separation compared with the cylindrical model because a secondary circulation develops in the vortex tube. Validation of a previous experimental study that used a cylindrical vortex tube has also been performed in this research.

Key words: Vortex tube; Divergent hot tube; Numerical simulation; Energy separation.

1. INTRODUCTION

The vortex tube is a simple device, without any moving parts, that separates a pressurized flow of air (or any inert gas) into hot and cold streams. Compressed air enters tangentially into the vortex tube, where it splits into two lower pressure streams, the peripheral vortex and the inner vortex. The hot stream rotates near the outer radius of the tube while the cold stream flows at the center of the tube. The hot, outer shell of the compressed gas escapes through the conical valve at the end of the tube. The remaining gas returns in an inner vortex and leaves through the cold exit orifice located at the other end of the tube near the inlet. This behavior is schematically illustrated in Fig. 1. There are various explanations for this behavior of the vortex tube. One explanation is that, owing to centrifugal force, the outer air is under higher pressure than the inner air. The temperature of the outer air is, therefore, higher than that of the inner air. Another explanation is that as both vortices have the same angular velocity and direction, the inner vortex loses angular momentum. This decrease in angular momentum is transferred to the outer vortex as kinetic energy, resulting in separated flows of hot and cold gas.

.

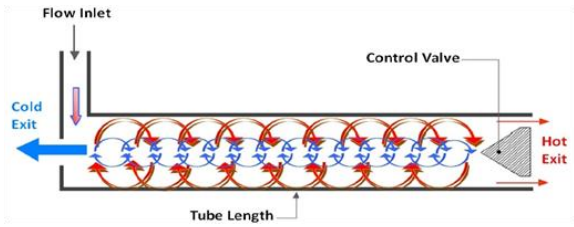

Figure 1. Schematic drawing of a vortex tube operational mechanism

French physicist Georges J. Ranque invented the vortex tube in 1933 [1]. Later, German physicist Rudolf Hilsch improved the design and published a widely read paper in 1947 on the device [2]. This device is, therefore, known as the Ranque-Hilsch vortex tube, as well. Although the device is geometrically simple, the phenomenon occurring in the tube is quite complex. A great amount of research has been dedicated to understanding the energy separation phenomenon in the Ranque-Hilsch vortex tube. Kurosaka stated that the temperature separation is a result of acoustic streaming effect [3]. Stephan et al. maintained that Gortler vortices form on the inside wall of the tube and drives the fluid motion [4]. An imbedded secondary circulation was discussed by Ahlborn and Gordon [5]. A CFD model of the vortex tube was employed by Aljuwayhel et al. [6] to understand the fundamental processes that cause the power separation inside the vortex tube. Behera et al. [7] investigated the effect of the number of nozzles on energy separation both experimentally and using a numerical CFD model. Skye et al. [8] made a comparison between the performance predicted by a computational fluid dynamic (CFD) model and experimental measurements taken using a commercially available vortex tube. Chang et al. [9] used the surface tracing method to carry out an experiment on the internal flow phenomena and to show the stagnation position in a vortex tube. Eiamsa-ard and Promvonge [10] utilized a CFD model to investigate the flow field and the temperature separation behavior. Pinar et al. [11] used the Taguchi method to obtain the optimal number of nozzles for the vortex tube. Xue et al. [12] studied pressure gradient, viscosity and turbulence, secondary circulation, and acoustic streaming in the vortex tube. Using a three-dimensional CFD model, Shamsoddini and Hossein Nezhad [13] analyzed the flow and heat transfer mechanism in the vortex tube. In order to investigate the variation of velocity, pressure, and temperature

inside a vortex tube, Akhesmeh et al. [14] developed a three-dimensional CFD model. Bramo and Pourmahmoud [15] numerically examined the effect of length-to-diameter ratio (L/D) and stagnation point position on temperature separation. Pourmahmoud et al. [16, 17] analyzed the effect of the number and the shape of nozzles on vortex tube behavior. They found that helical nozzles lead to higher swirl velocity and, hence, to greater temperature difference, as compared to straight nozzles. Earlier research showed that using a divergent hot tube compared with the cylindrical one improves the cooling performance of the vortex tube. Raiskii and Tankel [18] conducted an experimental study on energy separation of a typical vortex tube by using a divergent piece to form a part of the hot tube and reported that the typical vortex tube could improve the performance of the cylindrical one. Gulyaev et al. [19] found that replacing the cylindrical hot tube by a 2.3° divergent hot tube enhances the refrigeration capacity of the device. Takahama and Yokosowa [20] employed a divergent hot tube and reported its cooling performance to be higher than that of a cylindrical one of the same length. Chang et al. [21] investigated the effect of the divergent hot tube on temperature separation in an experimental study and found that the 4° divergent vortex tube provided the highest temperature reduction and that any increase or decrease in this critical angle causes the cooling performance of the vortex tube to decline.

In this paper, the numerical study focuses on disclosing the effect of the divergent hot tube on temperature separation. A numerical simulation is carried out to obtain the specified range of angles that improves the cooling performance of the divergent vortex tube compared with the cylindrical one.

2. CFD MODEL

The CFD model used in this study is based on that employed by Skye et al. [8]. It should be mentioned that the experimental device used by Skye et al. [8] was an Exair™ 708 slpm vortex tube. The geometrical properties of the device are provided in Table 1. The nozzle of the vortex tube consisted of six straight slots. In their work, Skye et al. [8] also numerically analyzed the vortex tube behavior using a two-dimensional (2D) model. However, the complex compressible turbulent flow inside the vortex tube necessitates an analysis of such patterns in 3D models.

Table 1. Geometric measurements of the vortex tube used in Skye *et al.*'s [8] experiment

Measurement	Value
Working tube length	106 mm
Working tube I.D.	11.4 mm
Nozzle height	0.97 mm
Nozzle width	1.41 mm
Nozzle total inlet area (A_n)	8.2 mm^2
Cold exit diameter	6.2 mm
Cold exit area	30.3 mm^2
Hot exit diameter	11 mm
Hot exit area	95 mm^2

The model used in the present study simulates a vortex tube having the same geometrical properties as that used in Skye et al.'s [8] experimental research. In order to reduce the computations, only a 60° sector of the flow domain in the CFD model is considered, since the models are assumed to be rotational periodic. Figure 2 demonstrates the 3D model.

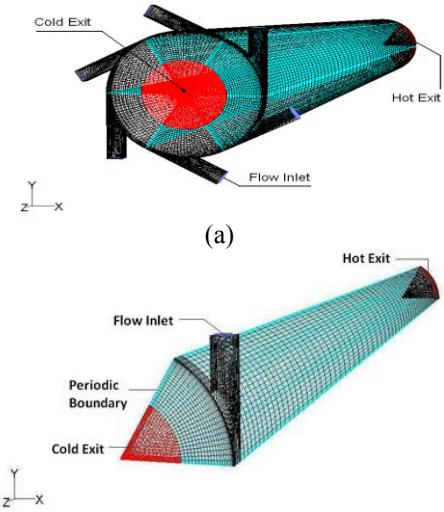

Figure 2. a) 3D CFD model of vortex tube with six straight nozzles b) a sector of the CFD model.

The boundary conditions in this numerical work are based on the experimental findings of Skye et al. [8], as follows:

(1) At the nozzle inlets, compressed air is modeled as mass flow inlet, with specified total mass flow rate at 8.35 gr/ s and stagnation temperature fixed at 294.2 K.

(2) At the cold outlet, the static pressure was fixed at the experimental measurement pressure.

(3) At the hot outlet, pressure is adjusted so as to vary the cold mass fraction.

(4) The wall of the vortex tube is assumed to be insulated and with no slip conditions.

3. GOVERNING EQUATIONS

The numerical simulation of the vortex tube flow field, as considered in this paper, has been created using FLUENT™ software package and is assumed to be a three-dimensional and steady model. Flow is considered to be compressible and turbulent, for which the standard k-ε turbulence model is employed. The renormalization group (RNG) k-ε turbulence model and the Reynolds stress equations were examined, as well. However, these two models could not be made to converge for this simulation. Bramo and Pourmahmoud [15] stated that the k-ε model is preferred to be used for simulating the turbulence in the vortex tube, since its numerical results exhibit better agreement with the experimental data. The governing equations for fluid flow are as follows:

-continuity equation:

$$\frac{\partial}{\partial x_j}(\rho u_j) = 0 \tag{1}$$

-momentum equation:

$$\frac{\partial}{\partial x_j}(\rho u_i u_j) = -\frac{\partial p}{\partial x_i} + \frac{\partial}{\partial x_j}\left[\mu\left(\frac{\partial u_i}{\partial x_j} + \frac{\partial u_j}{\partial x_i} - \frac{2}{3}\delta_{ij}\frac{\partial u_k}{\partial x_k}\right)\right] + \frac{\partial}{\partial x_j}(-\overline{\rho u_i' u_j'}) \tag{2}$$

-energy equation:

$$\frac{\partial}{\partial x_i}\left[u_i \rho\left(h + \frac{1}{2}u_j u_j\right)\right] = \frac{\partial}{\partial x_j}\left[k_{eff}\frac{\partial T}{\partial x_j} + u_i(\tau_{ij})_{eff}\right] \tag{3}$$

$$k_{eff} = K + \frac{c_p \mu_t}{\mathrm{Pr}_t}$$

As the working fluid is assumed to be an ideal gas, the state equation is necessary to show the compressibility effect, which is as follows:

$$p = \rho RT \tag{4}$$

The turbulence kinetic energy (k) and the rate of dissipation (ε) are obtained from the following equations:

$$\frac{\partial}{\partial t}(\rho k)+\frac{\partial}{\partial x_i}(\rho k u_i)=\frac{\partial}{\partial x_j}[(\mu+\frac{\mu_t}{\sigma_k})\frac{\partial k}{\partial x_j}]+G_k+G_b-\rho\varepsilon-Y_M \tag{5}$$

$$\frac{\partial}{\partial t}(\rho\varepsilon)+\frac{\partial}{\partial x_i}(\rho\varepsilon u_i)=\frac{\partial}{\partial x_j}[(\mu+\frac{\mu_t}{\sigma_\varepsilon})\frac{\partial\varepsilon}{\partial x_j}]+C_{1\varepsilon}\frac{\varepsilon}{k}(G_k+C_{3\varepsilon}G_b)-C_{2\varepsilon}\rho\frac{\varepsilon^2}{k} \tag{6}$$

where G_k, G_b, and Y_M represent the generation of turbulent kinetic energy due to the mean velocity gradients, the generation of turbulent kinetic energy due to buoyancy, and the contribution of the fluctuating dilatation in compressible turbulence to the overall dissipation rate, respectively; $C_{1\varepsilon}$ and $C_{2\varepsilon}$ are constants. These default values have been determined from experiments with air and water for fundamental turbulent shear flows including homogeneous shear flows and decaying isotropic grid turbulence. They have been found to work fairly well for a wide range of wall-bounded and free shear flows. σk and σε are the turbulent Prandtl numbers for k and ε. The turbulent viscosity, μt, is computed as follows:

$$\mu_t = \rho C_\mu \frac{k^2}{\varepsilon} \tag{7}$$

where C_μ is a constant. The model constants $C_{1\varepsilon}$, $C_{2\varepsilon}$, C_μ, σ_k, and σ_ε have the following default values: $C_{1\varepsilon}$ = 1.44, $C_{2\varepsilon}$ = 1.92, C_μ = 0.09, σ_k = 1.0, σ_ε = 1.3. Finite volume method with a 3D structured mesh is applied to the governing equations, which is one of the numerical approaches to describe complex flow patterns in the vortex tube. Inlet air is considered as a compressible working fluid, where its specific heat, thermal conductivity and dynamic viscosity are taken to be constant during the numerical analysis procedure. Second order upwind scheme is utilized to discretize convective terms, and SIMPLE algorithm is used to solve the momentum and energy equations simultaneously. Because of highly non-linear and coupling virtue of the governing equations, lower under-relaxation factors ranging from 0.1 to their default amount are taken for the pressure, density, body forces, momentum, k, ε , turbulent viscosity and energy components to ensure the stability and convergence of the iterative calculations.

4. RESULTS AND DISCUSSION

4.1 Grid independency

In order to show grid independency of the results, different average unit cell volumes in the model have been analyzed. The two main parameters studied are variation of total temperature difference and maximum swirl velocity, as shown in Fig. 3. Decreasing the unit cell volume size below 0.0257 mm^3, corresponding to 0.287 million cells in the model, does not result in a considerable difference in the two parameters.

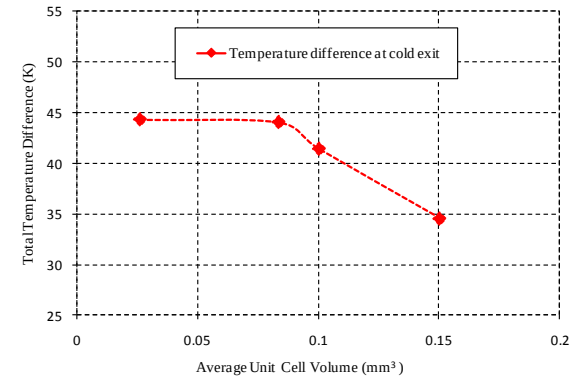

(a)

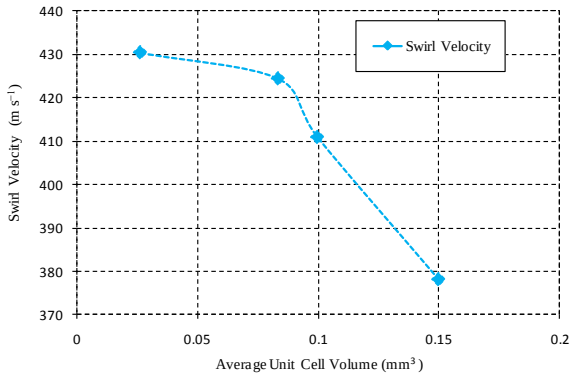

(b)

Figure 3. Grid size dependence on a) total temperature difference and b) maximum swirl velocity at different average unit cell volumes.

4.2 Validation

Temperature separation results obtained from CFD simulation in this study are compared with the experimental results of Skye et al. [8] as shown in Fig. 4. Figure 4 (a) exhibits the good agreement between cold temperature difference ($\Delta T_{i,c}$) obtained in this article and Skye et al.'s [8] results. As compared with Skye et al.'s [8] computational results, the present results were closer to the experimental results. As regards hot temperature separation ($\Delta T_{i,h}$), the numerical results of both Skye et al. [8] and the present study are very close to the experimental results, as displayed in Fig. 4 (b). The maximum $\Delta T_{i,c}$ is obtained at a cold mass fraction of about 0.3 in both the experiment and the CFD model. An increase in the cold mass fraction leads to an increase in the hot exit temperature difference. At the cold mass fraction 0.81, the maximum hot exit temperature difference was observed.

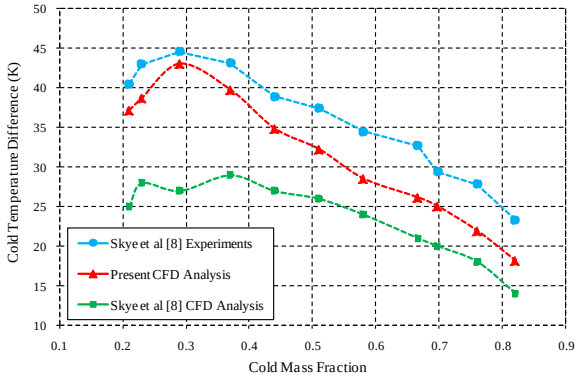

(a)

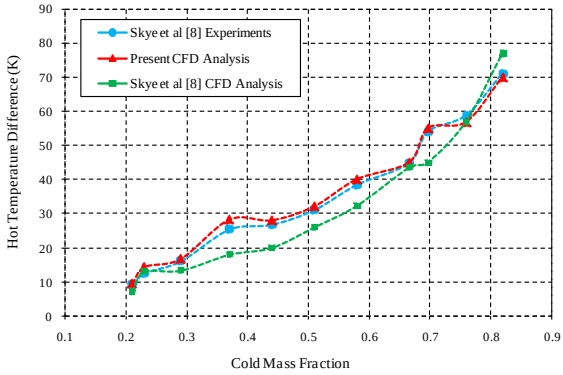

(b)

Figure 4. Comparison of the present CFD model and the experimental results with regard to a) cold temperature difference and b) hot temperature difference.

4.3 Cylindrical vortex tube investigation

CFD analysis has been conducted to investigate the variation of velocity components, total pressure, and total temperature on radial profiles at three axial locations (Z/L= 0.1, 0.4, 0.7) at cold mass fraction 0.3 to understand flow characteristics within the cylindrical vortex tube. In Figs. 5 and 6, the radial profiles for the swirl velocity and axial velocity at Z/L= 0.1, 0.4, and 0.7 are provided. It can be observed that the swirl velocity has greater magnitude than the axial velocity. According to these figures, the magnitudes of swirl velocity and axial velocity decrease rapidly as we move from the inlet to the hot outlet. The radial profile of swirl velocity indicates a free vortex near the wall. On the other hand, another, forced, vortex is formed in the core which is consistent with the findings of Kurosaka [3] and Gustol [22]. Also, the profiles obtained for the swirl velocity and axial velocity at different axial locations are in good agreement with the observations of Gutsol [22] and Behera et al. [7].

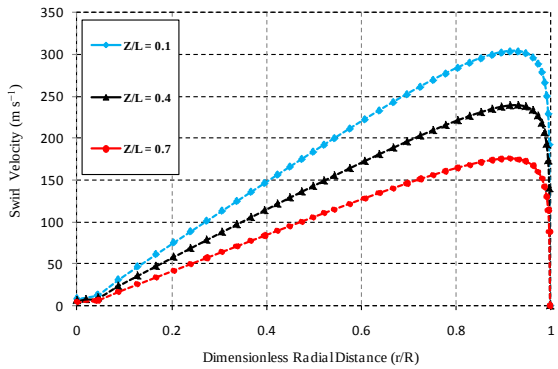

Figure 5. Radial profile of swirl velocity at different axial locations for α=0.3.

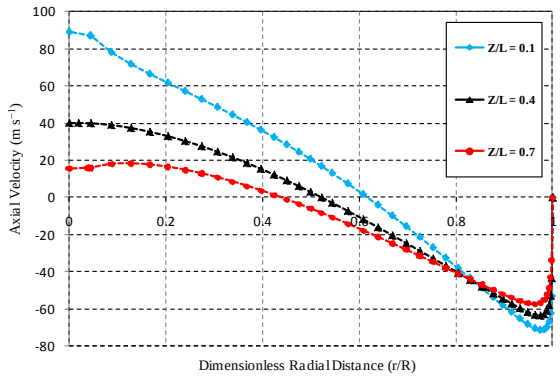

Figure 6. Radial profile of axial velocity at different axial locations for α=0.3

The total temperature variations at three axial locations Z/L= 0.1, 0.4, and 0.7 are presented in Fig. 7. The figure shows that maximum total temperature occurred near the periphery of the tube wall. Also, the low temperature zone in the core coincides with the negligible swirl velocity zone. Figure 8 shows the total pressure variations at three axial locations Z/L= 0.1, 0.4 and 0.7. Total pressure increases radially in all Z/L cross-sections as shown in Fig. 8. The maximum total pressure is, therefore, observed near the periphery of the tube wall and the minimum occurs in the core layers. Pressure difference between peripheral layers and core layers decreases as distance from the inlet increases.

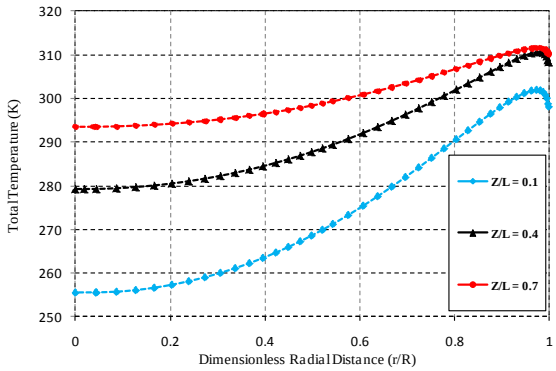

Figure 7. Radial profile of total temperature at different axial locations for α=0.3.

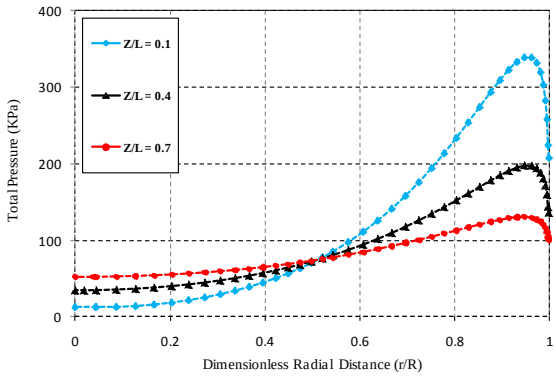

Figure 8. Radial profile of total pressure at different axial locations for α=0.3.

The contours of total temperature for cold mass fraction 0.3 in cylindrical vortex tube are displayed in Fig. 9. It can be clearly seen that the peripheral flow is warm and the core flow is cold. Furthermore, increase of temperature is observed in the radial direction. For a cold mass fraction of about 0.3, the cylindrical vortex tube gives the maximum hot gas

temperature of 311.5 [K] and the minimum cold gas temperature of 250.24 [K].

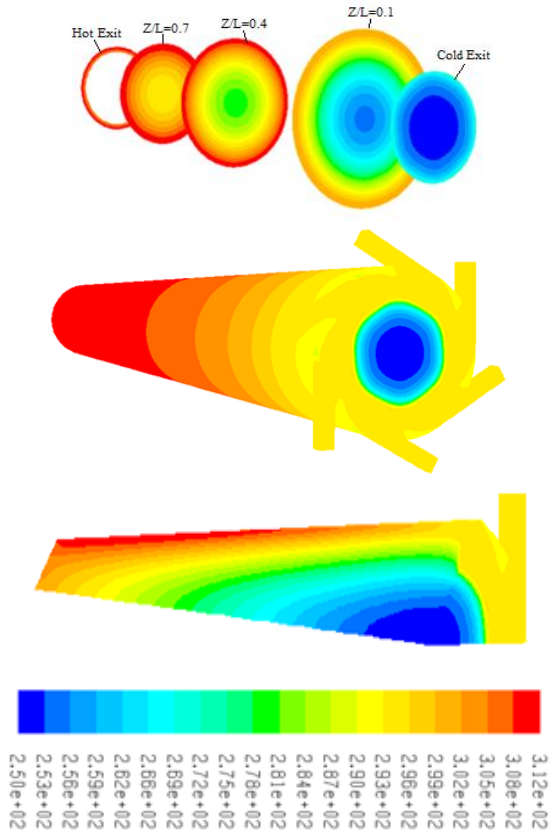

Figure 9. Contours of total temperature at Ti= 294.2 K.

4.3 The effect of divergent hot tube

The geometry of the vortex tube affects its cooling performance. Many researchers have, therefore investigated the effect of shape and number of inlet nozzles, the length and diameter of the working tube, etc. One of the significant geometrical parameters, which has not been much studied, is the divergence angle of the hot tube. In recent years, a few experimental works have been carried out on the effect of the divergence angle of the hot tube (Chang et al., [21]), but the lack of numerical investigation is felt. In order to investigate the effect of using a divergent hot tube, the above-mentioned simulated model has been utilized in this study. All parameters, except the angle of divergence have been kept constant. The angle β is defined as the deviation from the cylindrical model (β= 0°) as shown in Fig. 10.

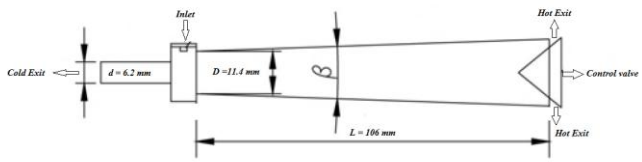

Figure 10. Schematic of vortex tube with divergent hot tube**.**

To examine the effect of the divergent hot tube, very small degrees (β=0°, 0.2°, 0.4°, 0.6°, 0.8°, and 1°) were first simulated. The numerical results obtained from these simulations are indicated in Fig. 11. The cold temperature difference for different cold mass fractions, i.e., 0.3, 0.4, 0.5, and 0.6, are presented in this figure for the above-mentioned range of angles. The figure shows that the angle β= 0.4° is a threshold before which the change of cold temperature difference is steep but after which the change of temperature difference is negligible. Moreover, from this diagram it is understood that using a divergent hot tube increases the temperature difference for cold mass fractions greater than about 0.4.

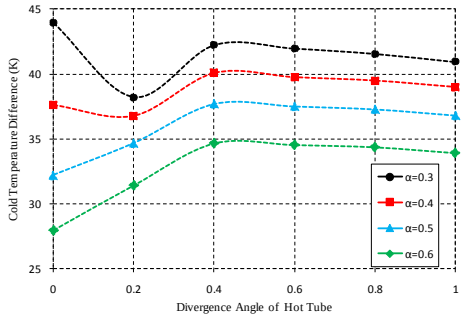

Figure 11. Effect of the angle of divergent hot tube on cooling performance of vortex tube.

In addition to the above-mentioned work, a numerical simulation was carried out for β= 1°, 2°, 3°, 4°, and 6° to investigate the temperature separation performance at the cold and hot outlets at different cold mass fractions. These results are depicted in Figs. 12 and 13. Figure 12 shows that the maximum cold temperature difference occurs at cold mass fraction 0.3 in the cylindrical model (β= 0°). It was also found that at β=1°, 2°, and 3°, the cooling performance of the vortex tube was better than that at β= 0° at cold mass fractions greater than about 0.4. With the increase in the angle from β= 4° to β= 6°, there is an obvious decrease in the cooling performance compared with that at β= 0. These results can be elucidated on the basis of the statement by Shannak [23] as follows: at cold mass fractions higher than 0.4, the energy separation performance is due to the more dominant role of viscous resistance, friction, and the separation flow or secondary circulation flow. The divergence of the angle from the cylindrical model (β= 0) reduces the swirling velocity of the gas stream in the hot tube and brings about a decrease in the friction loss and the internal viscous loss, which leads to an increase in the energy separation. But, when the angle of the divergent hot tube increases more, the secondary circulation flow will develop in the tube, which causes a decrease in temperature separation. At cold mass fractions lower than 0.4, the energy separation performance is due to the more dominant role of swirl velocity. In this range of cold mass fractions, the swirl velocity is large enough to overcome the viscous resistance. Therefore, the cylindrical model with the largest swirl velocity exhibits the maximum cold temperature difference.

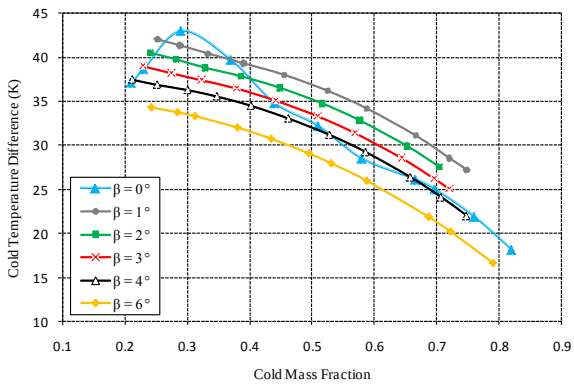

Figure 12. Influence of the angle of divergent hot tube on the cold temperature difference.

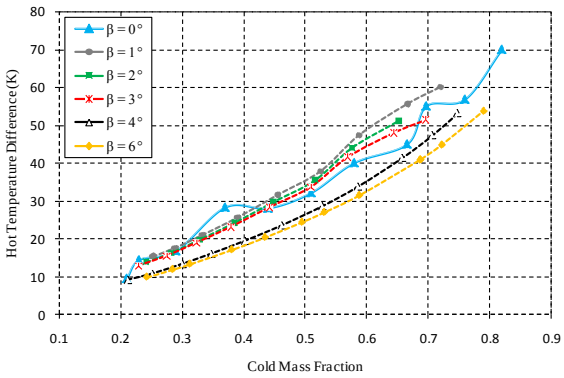

Figure 13. Influence of the angle of divergent hot tube on the hot temperature difference.

In order to demonstrate the effect of divergence angle change on radial profiles of swirl velocity, the profiles at three axial locations (Z/L= 0.1, 0.4, 0.7) at cold mass fractions 0.3 and 0.7 (to present profiles for cold mass fractions lower than and greater than 0.4, respectively) were analyzed, the diagrams of which are depicted in Figs. 14 and 15. The diagrams show that the swirl velocity of the gas stream decreases as the angle increases in each radial profile. Also, for all angles, as we move towards the hot exit, the swirl velocity decreases.

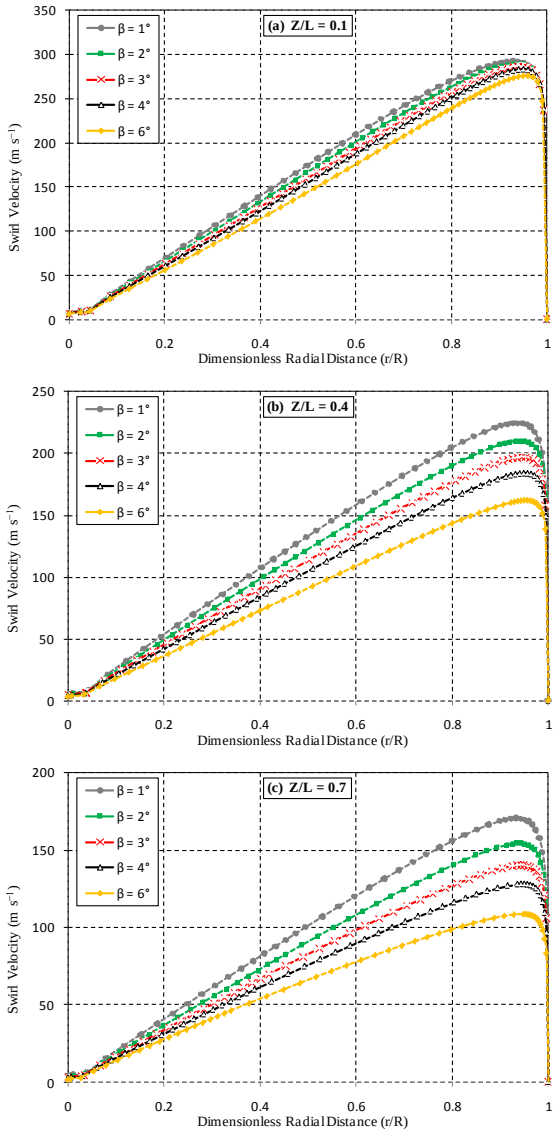

Figure 14. Radial profile of swirl velocity at different axial locations for α=0.3.

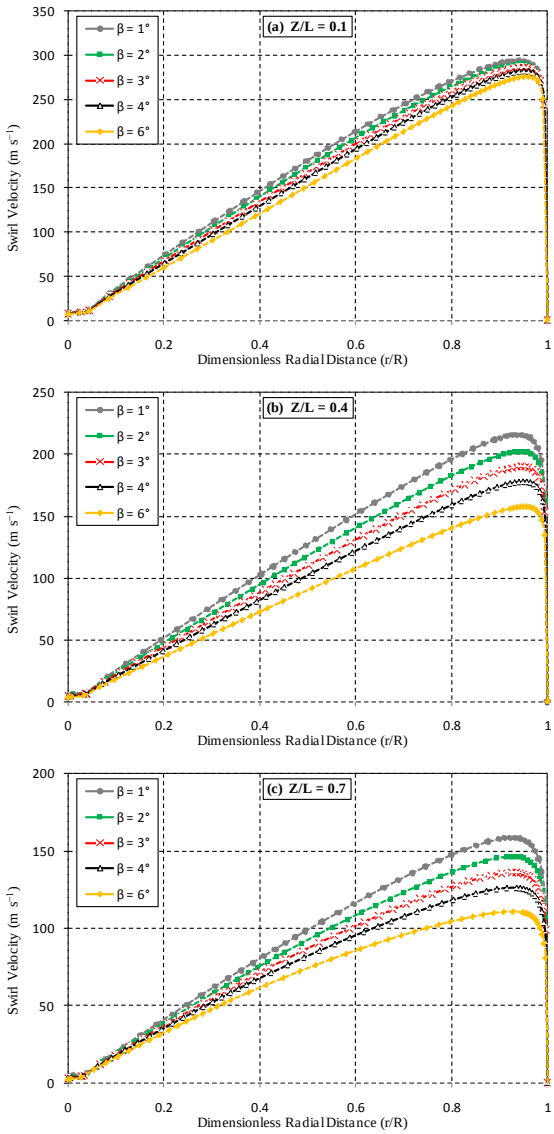

Figure 15. Radial profile of swirl velocity at different axial locations for α=0.7.

In Figs. 16 and 17, the radial profiles for the axial velocity at Z/L= 0.1, 0.4, and 0.7 at cold mass fractions 0.3 and 0.7 are provided. It can be observed that the axial velocity has a lower magnitude than the swirl velocity. Moreover, both velocity components of the stream dwindle as it moves on to the hot end exit.

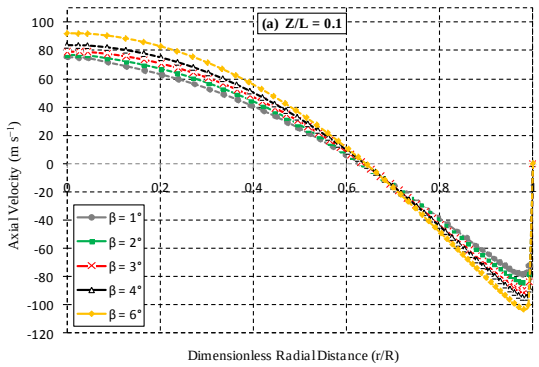

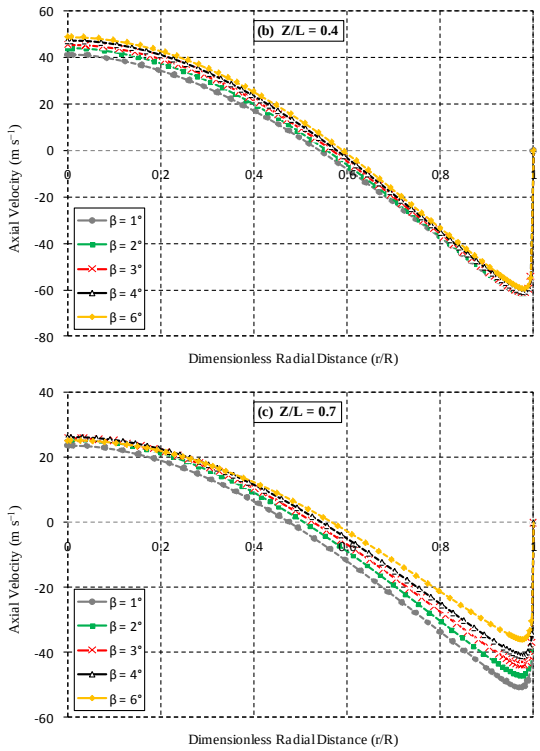

Figure 16. Radial profile of axial velocity at different axial locations for α=0.3.

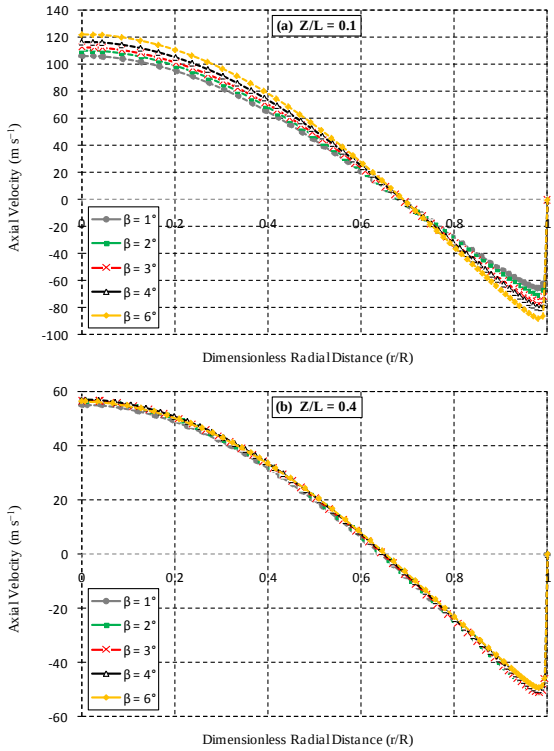

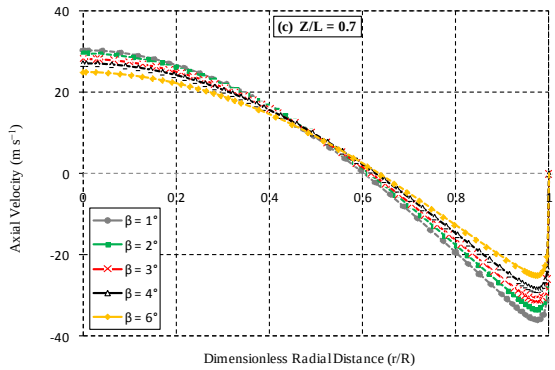

Figure 17. Radial profile of axial velocity at different axial locations for α=0.7.

Figures 18 and 19 show the total pressure variations for different inlet gas temperatures at the three axial locations Z/L= 0.1, 0.4, and 0.7 at cold mass fractions 0.3 and 0.7. As was the case with the cylindrical working tube, there is a radial increase in total pressure in all Z/L cross-sections. Therefore, the maximum total pressure occurs near the periphery of the tube wall in the divergent vortex tube and the minimum occurs in the core layers. Pressure difference between peripheral layers and core layers decreases as we move away from the inlet.

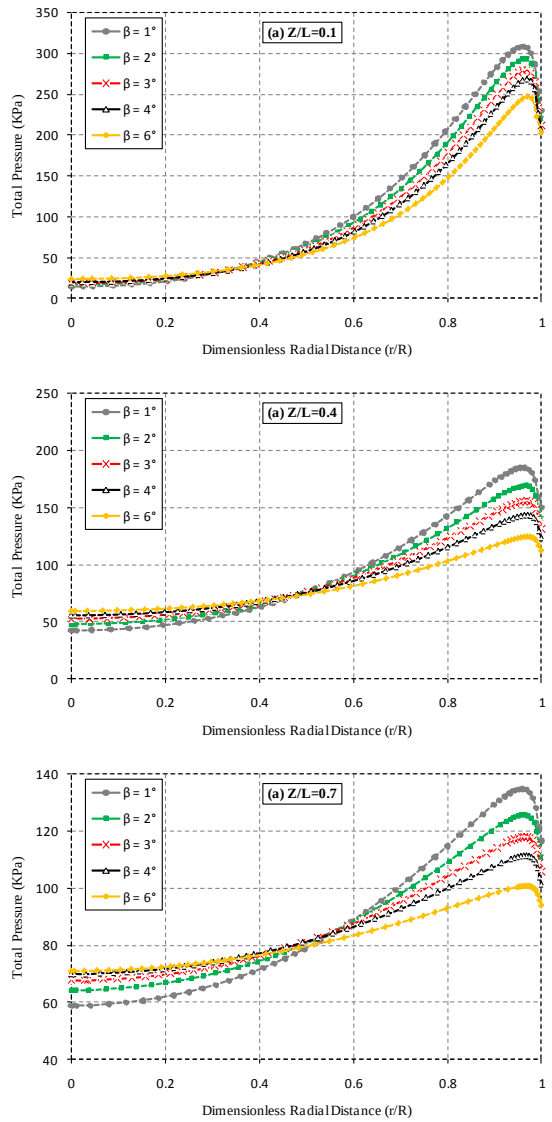

Figure 18. Radial profile of total pressure at different axial locations for α=0.3.

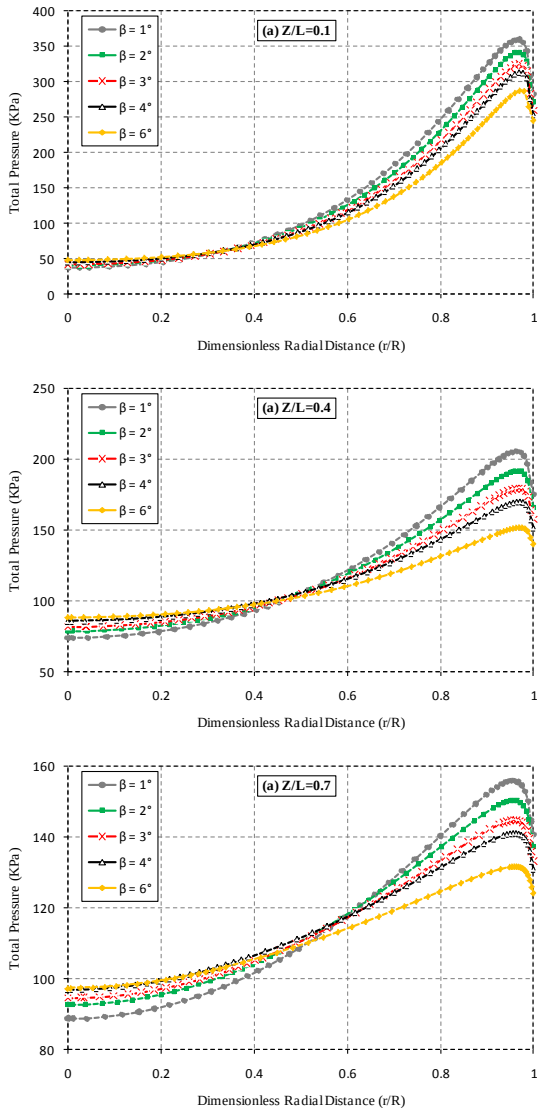

Figure 19. Radial profile of total pressure at different axial locations for α=0.7.

In Figs. 20 and 21, the radial profiles for the total temperature at Z/L= 0.1, 0.4, and 0.7 at cold mass fractions 0.3 and 0.7 are provided. We can observe that maximum total temperature occurred near the periphery of the tube wall in all models. Also, the low temperature zone in the core coincides with the negligible swirl velocity zone.

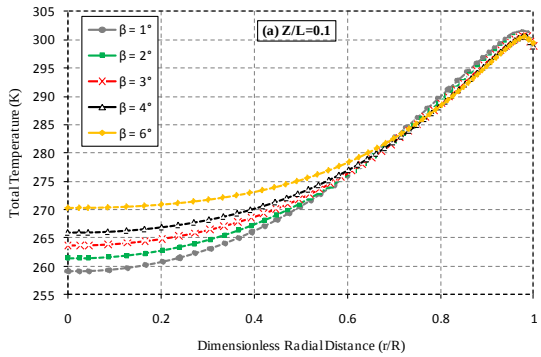

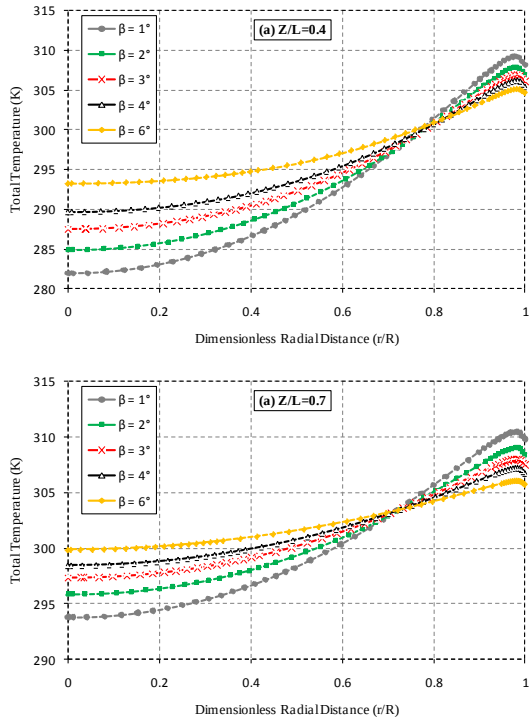

Figure 20. Radial profile of total temperature at different axial locations for α=0.3.

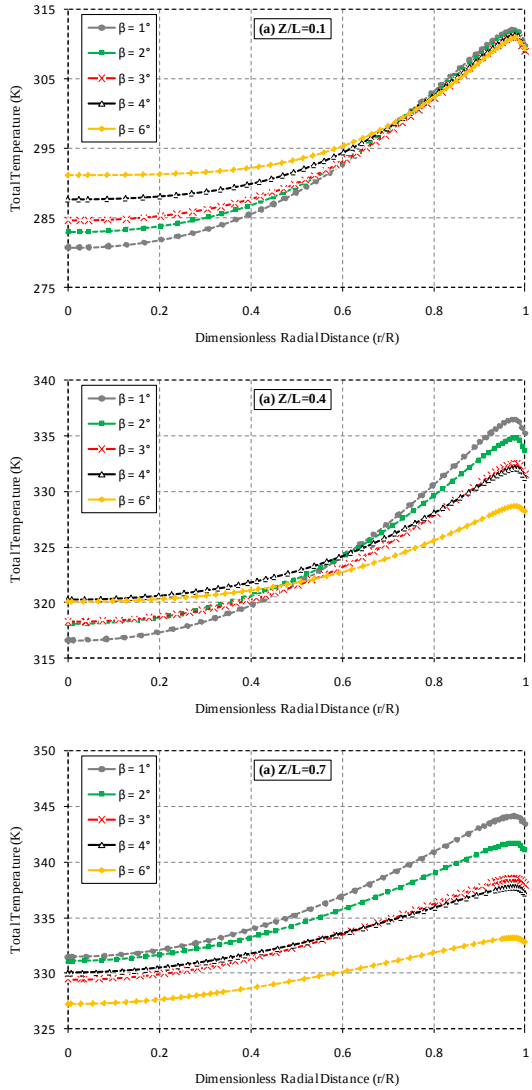

Figure 21. Radial profile of total temperature at different axial locations for α=0.3.

5. CONCLUSIONS

In this study, a 3D CFD model was created to analyze the temperature separation in a cylindrical vortex tube. This model is based on the experimental study by Skye et al. [8]. The model was developed using a three-dimensional, steady model that utilized the standard k-ε turbulence equations. There was good agreement between the CFD results and the measured experimental data. The numerical model is capable of obtaining swirl velocity and axial velocity components of the flow, which are difficult to obtain experimentally. The analysis showed that the maximum $\Delta T_{i,c}$ is obtained at a cold mass fraction of about 0.3 and that the maximum $\Delta T_{i,h}$ at cold mass fraction 0.8 was observed in both the experimental study and the CFD model. According to these results, the swirl velocity magnitude is higher than axial and radial velocities.

In addition to the above-mentioned work, the effect of using a divergent hot tube on energy separation in a vortex tube was simulated, where all the parameters were kept constant except for the divergence angle. The numerical results indicated that the cooling performance of the vortex tube can be improved by utilizing a divergent hot tube at cold mass fractions higher than 0.4. However, this improvement can be achieved as long as the divergence angle does not exceed 4°.

NOMENCLATURES

C_p	Specific heat at constant pressure, j/(kg.K)
D	Diameter of vortex tube, mm
h	Mass-averaged enthalpy, j/kg
k	Turbulence kinetic energy, m^2/ s^2
K	Thermal conductivity, w/(m.K)
L	Length of vortex tube, mm
p	Pressure, N/m^2
Pr	Prandtl number
r	Radial distance from the centerline, mm
R	Radius of vortex tube, mm
T	Temperature, K
u_i	Velocity component, m/s
Z	Axial length from nozzle cross section, mm

GREEK SYMBOLS

α	Cold mass fraction
β	Divergence angle of the hot tube
δ_{ij}	Kronecker delta
ε	Turbulence dissipation rate, m^2/s^3
ΔT	Temperature difference, K
ρ	Density, kg/ m^3
μ	Dynamic viscosity, kg/(m.s)
μ_t	Turbulent viscosity, kg/(m.s)
σ	Stress, N/m^2
τ	Shear stress, N/m^2
τ_{ij}	Stress tensor components

SUBSCRIPTS

i	Inlet
c	Cold
h	Hot

6. REFERENCES

1. G.J. Ranque, Experiments on expansion in a vortex with simultaneous exhaust of hot air and cold air, J. Phys. Radium (Paris), Vol. 4, pp. 112–115, 1933.
2. R. Hilsch, The use of expansion of gases in a centrifugal field as a cooling process, Rev. Sci. Instrum, Vol. 18, pp. 108–113, 1947.
3. M. Kurosaka, Acoustic streaming in swirling flows and the Ranque-Hilsch vortex-tube effect, J. Fluid Mech, Vol. 124, pp. 139–172, 1982.
4. K. Stephan, S. Lin, M. Durst, F. Huang and D. Seher, An investigation of energy separation in a vortex tube, Int. J. Heat Mass Transfer, Vol. 26, pp. 341–348, 1983.
5. B.K. Ahlborn and J.M. Gordon, The vortex tube as a classic thermodynamic refrigeration cycle. J. Appl. Phys, Vol. 88, pp. 3645–3653, 2000.
6. N.F. Aljuwayhel, G.F. Nellis and S.A. Klein, Parametric and internal study of the vortex tube using a CFD model, Int. J. Refrigeration, Vol. 28, pp. 442–450, 2005.
7. U. Behera, P.J. Paul, S. Kasthurirengen, R. Karunanithi, S. N. Ram, K. Dinesh and S. Jacob, CFD analysis and experimental investigations towards optimizing the parameters of Ranque– Hilsch vortex tube, Int. J. Heat Mass Transfer, Vol. 48, pp. 1961–1973, 2005.
8. H.M. Skye, G.F. Nellis and S.A. Klein, Comparison of CFD analysis to empirical data in a commercial vortex tube, Int. J. Refrigeration, Vol 29, pp. 71–80, 2006.
9. H.S. Chang, S.K. Chang, H.J. Ui and B.H.L. Lakshmana Gowda, Experimental and Numerical Studies in a Vortex Tube, J. Mech. Sci. Tech, Vol. 20, pp. 418–425, 2006.
10. S. Eisma-ard and P. Promvonge, Numerical investigations of the thermal separation in a Ranque-Hilsch vortex tube, Int. J. Heat Mass Transfer, Vol 50, pp. 821–832, 2007.
11. A.M. Pinar, O. Uluer and V. Kirmaci, Optimization of counter flow Ranque-Hilsch vortex tube performance using Taguchi method. Int. J. Refrigeration, Vol 32, pp. 1487–1494, 2009.
12. Y. Xue, M. Ajormandi and R. Kelso, A critical review of temperature separation in a vortex tube, J. Exp. Therm. Fluid Sci, Vol. 34, pp. 1367–1374, 2010.
13. R. Shamsoddini and A. Hossein Nezhad, Numerical analysis of the effects of nozzles number on the flow and power of cooling of a vortex tube. Int. J. Refrigeration, Vol. 33, pp. 774–782, 2010.
14. S. Akhesmeh, N. Pourmahmoud and H. Sedgi, Numerical study of the temperature separation in the Ranque-Hilsch vortex tube. Am. J. Eng. Appl. Sci, Vol 1, pp. 181–187, 2008.
15. A.R. Bramo and N. Pourmahmoud, CFD simulation of length to diameter ratio effect on the energy separation in a vortex tube. Therm. Sci, Vol 15, pp. 833–848, 2011.
16. N. Pourmahmoud, A. Hassan Zadeh, S.E. Rafiee and M. Rahimi, Three Dimensional Numerical Investigation of Effect of Convergent Nozzles on the Energy Separation in a Vortex Tube, International Journal of Heat and Technology, vol. 30(2), pp. 133-140, 2012.
17. N. Pourmahmoud, A. Hassan Zadeh and O. Moutaby, Numerical Analysis of the Effect of Helical Nozzles Gap on the Cooling Capacity of Ranque-Hilsch Vortex Tube, Int. J. Refrigeration, Vol. 35, pp. 1473–1483. 2012.

18. Y.D. Raiskii and L.E. Tankel,. Influence of vortex-tube saturation and length on the process of energetic gas separation. J. Eng. Phys, Vol 27, pp. 1578–1581, 1974.
19. A.I. Gulyaev, Investigation of conical vortex tubes, J. Eng. Phys, Vol 10, pp. 193–195, 1966.
20. H. Takahama and H. Yokosawa, Energy separation in vortex tube with a divergent chamber, J. Heat Transfer, Trans. ASME, Vol 103, pp.196–203, 1981.
21. K. Chang, Q. Li, , G. Zhou and Q. Li, Experimental investigation of vortex tube refrigerator with a divergent hot tube, Int. J. Refrigeration, Vol 34, pp. 322–327, 2011.
22. A.F. Gutsol, The Ranque effect. Phys. Usp, Vol 40, pp. 639–658, 1997.
23. B.A. Shannak, Temperature separation and friction losses in vortex tube. Heat Mass Transfer, Vol 40, pp. 779–785, 2004.